WATER RESOURCES RESEARCH, VOL. 49, 1782–1796, doi:10.1002/wrcr.20129, 2013

# Joint interpretation of sequential pumping tests in unconfined aquifers

Deqiang Mao,[1,2] Tian-Chyi J. Yeh,[2,3] Li Wan,[1] Jet-Chau Wen,[4] Wenxi Lu,[5] Cheng-Haw Lee,[3] and Kuo-Chin Hsu[3]

Received 24 April 2012; revised 29 January 2013; accepted 5 February 2013; published 8 April 2013.

[1] In this study, we developed a stochastic estimator for characterizing the hydraulic heterogeneity in both unsaturated and saturated zones of unconfined aquifers using transient drawdown data from sequential pumping tests. This estimator was built upon the successive linear estimator by Yeh et al. (1996), the simultaneous successive linear estimator by Xiang et al. (2009), and the 3-D finite element program for flow and transport through heterogeneous media by Srivastava and Yeh (1992). The estimator was tested afterward using simulated data sets of sequential pumping tests in a synthetic unconfined aquifer where saturated conductivity, specific storage, saturated water content, and pore-size distribution parameter vary spatially in three dimensions. Test results show that the estimator is able to produce parameter fields that capture the overall 3-D pattern of the true heterogeneous parameter fields. We subsequently validated the estimated parameter fields by assessing their ability to predict drawdowns during an independent pumping test, which was not used during the estimation phase. Results of the validation show that the predicted drawdowns based on the estimated heterogeneous parameter fields are in close agreement with the true drawdowns. In addition, predicted drawdowns based on the parameter fields from the joint interpretation are superior to those based on the parameters estimated from the homogeneous conceptual model. Lastly, while many field experiments are necessary to fully assess the robustness of this estimator and sequential pumping tests, results of this study suggest they are a promising characterization technique for unconfined aquifers.

**Citation:** Mao, D., T.-C. J. Yeh, L. Wan, J.-C. Wen, W. Lu, C.-H. Lee, and K.-C. Hsu (2013), Joint interpretation of sequential pumping tests in unconfined aquifers, *Water Resour. Res.*, *49*, 1782–1796, doi:10.1002/wrcr.20129.

## 1. Introduction

[2] Detailed characterization of inherent aquifer heterogeneity is necessary for an accurate assessment of groundwater resource and pollution problems. Traditional characterization approaches have adopted homogeneous conceptual models that assume aquifer homogeneity and have attempted to derive effective hydraulic parameters based on drawdowns from a single pumping test, for example, those by *Theis* [1935] and *Cooper and Jacob* [1946] for confined aquifers and those by *Boulton* [1963], *Dagan* [1967], *Brutsaert* [1970], *Streltsova* [1972a, 1972b], *Neuman* [1972], *Lakshminarayana and Rajagopalan* [1978], *Moench* [1995], *Mathias and Butler* [2006], and *Mishra and Neuman* [2010] for unconfined aquifers. Recent numerical, sandbox, and field experiments by *Wu et al*. [2005], *Straface et al*. [2007], *Xiang et al*. [2009], *Wen et al*. [2010], *Huang et al*. [2011], and *Berg and Illman* [2011b] however questioned the representativeness of the estimates from these conventional approaches.

[3] Aquifer characterization built upon heterogeneous conceptual models is also not immune from problems. *Huang et al*. [2011], using numerical and field experiments, demonstrated that the heterogeneous transmissivity distribution estimated from many observation wells during a single pumping test could vary with the location of the pumping well (i.e., scenario-dependent estimates). More critically, they showed that predicted drawdowns based on this type of heterogeneous characterization approaches are biased if the stress location is different from the pumping well location used in the characterization.

[4] For the last decade, sequential pumping tests, multi-well interference tests, or hydraulic tomography (HT) have

[1]School of Water Resources and Environmental Science, China University of Geosciences, Beijing, China.
[2]Department of Hydrology and Water Resources, The University of Arizona, Tucson, Arizona, USA.
[3]Department of Resources Engineering, National Cheng Kung University, Tainan, Taiwan.
[4]Department of Safety, Health and Environmental Engineering, Research Center for Soil and Water Resources and Natural Disaster Prevention, National Yunlin University of Science and Technology, Touliu, Yunlin, Taiwan.
[5]College of Environment and Resources, Jilin University, Changchun, Jilin, China.

Corresponding author: D. Mao, Department of Hydrology and Water Resources, The University of Arizona, Tucson, AZ 85721, USA. (deqiang@email.arizona.edu)


0043-1397/13/10.1002/wrcr.20129

been the subject of active research to characterize the spatial distributions of hydraulic parameters. They include numerical studies [e.g., *Gottlieb and Dietrich*, 1995; *Yeh and Liu*, 2000; *Bohling et al*., 2002; *Zhu and Yeh*, 2005, 2006; *Fienen et al*., 2008; *Ni and Yeh*, 2008; *Castagna and Bellin*, 2009; *Xiang et al*., 2009; *Liu and Kitanidis*, 2011], followed by laboratory sandbox studies [e.g., *Liu et al*., 2002; *Brauchler et al*., 2003; *Illman et al*., 2007; *Liu et al*., 2007; *Illman et al*., 2008; *Yin and Illman*, 2009; *Illman et al*., 2010; *Berg and Illman*, 2011a; *Illman et al*., 2012] and then experimental field studies [e.g. *Bohling et al*., 2007; *Li et al*., 2007; *Straface et al*., 2007; *Cardiff et al*., 2009; *Illman et al*., 2009; *Berg and Illman*, 2011b; *Brauchler et al*., 2011; *Huang et al*., 2011]. All these studies have consistently shown that transient HT can identify not only the pattern of the heterogeneous hydraulic conductivity field but also the variation of specific storage. More importantly, the hydraulic property fields estimated by HT have been demonstrated to yield much better predictions of flow and transport processes than conventional characterization approaches [see *Yeh and Zhu*, 2007; *Ni et al*., 2009; *Huang et al*., 2011; *Illman et al*., 2012]. Recent work by *Berg and Illman* [2011b] further substantiated the robustness of HT for a highly heterogeneous geological medium with a variance of log hydraulic conductivity of 5.4 and a vertical correlation scale of 0.15 m. Thus, the call for changing the way we collect and analyze data for characterization of aquifers by *Yeh and Lee* [2007] appears to be well founded.

[5] Most HT studies, however, have focused on confined aquifers and estimation of saturated hydraulic conductivity and specific storage. To the best of our knowledge, the only few HT applications associated with unconfined aquifers are the work done by *Zhu and Yeh* [2008], *Zhu et al*. [2011], *Cardiff et al*. [2009], and *Cardiff and Barrash* [2011]. In the work by *Cardiff et al*. [2009], they presented a potential-based inversion method for steady-state pumping tests in an unconfined aquifer. The method employs the Dupuit-Forchheimer assumption and neglects unsaturated flow.

[6] Subsequently, *Cardiff and Barrash* [2011] developed a 3-D transient HT approach for characterizing unconfined aquifers with a fast drainage response assumption. This assumption, in essence, ignores the effects of flow in the unsaturated zone above the water table, and pressure-dependent hydraulic conductivity and moisture release nature of unsaturated flow process during lowering the water table due to pumping. As a result, their method is limited to mapping hydraulic conductivity, specific storage, and specific yield of the aquifer. Furthermore, *Nwankwor et al*. [1984] and *Endres et al*. [2007] reported that models based on the fast drainage response assumption often produce unreasonably small values of the specific yield. Because of these issues, *Cardiff and Barrash* [2011] suggested that their model is most suitable for characterizing coarse-grained aquifers during short-temporal-scale pumping tests.

[7] By analyzing the transition of different water release mechanisms during pumping tests in unconfined aquifers and examining the cross correlation between heads and heterogeneities in aquifers, *Mao et al*. [2011], *Yeh et al*. [2012], and *Mao et al*. [2013] advocated that a multidimensional heterogeneous variably saturated flow model would provide a more realistic representation of the flow process during a pumping test in unconfined aquifers. They also suggested that the variability of unsaturated parameters, in general, does not significantly affect the observed head in saturated zones during pumping tests in unconfined aquifers.

[8] *Zhu and Yeh* [2008] and *Zhu et al*. [2011] developed an interpretation procedure based on the variably saturated flow model for sequential pumping tests in unconfined aquifers. Their results, however, are preliminary because of some technical issues, solution convergence, and other problems associated with computational efficiency. In this study, we continued the work by *Zhu and Yeh* [2008] and *Zhu et al*. [2011] to develop a versatile, stochastic, simultaneously successive linear estimator (SimSLE) based on the 3-D variably saturated flow model to jointly interpret drawdown data from sequential pumping tests in unconfined aquifers for characterizing the spatial distribution of aquifer properties. Numerical experiments were then used to test the estimator and spatial and temporal sampling strategies proposed by *Mao et al*. [2013a, 2013]. Furthermore, we evaluated these estimated parameter fields against those from the traditional approach based on the homogeneous assumption by predicting drawdowns during an independent pumping test.

## 2. Methodology

### 2.1. Equation for Variably Saturated Groundwater Flow

[9] Flow in an unconfined aquifer involves processes in saturated and unsaturated zones and dynamics of the water table. The following governing equation for flow through variably saturated media is a suitable candidate for describing the flow during pumping tests in unconfined aquifers [*Mao et al*., 2011]:

$$\nabla \cdot [K(h,\mathbf{x})\nabla(h+z)] + Q(\mathbf{x}_p) = [\omega S_S(\mathbf{x}) + C(h,\mathbf{x})]\frac{\partial h}{\partial t} \qquad (1)$$

subject to boundary and initial conditions

$$h|_{\Gamma_1} = h_1, \quad -K(\mathbf{x})\nabla(h+z)|_{\Gamma_2} = q, \quad h|_{t=0} = h_0, \qquad (2)$$

where $\nabla$ is the differential operator, $t$ is time, $\theta(h,\mathbf{x})$ represents the volumetric moisture content, and $z$ is the elevation. $h$ is the pressure head and is positive when the medium is saturated and negative when unsaturated. $Q(\mathbf{x}_p)$ is the pumping rate per unit volume at location $\mathbf{x}_p$. The saturation index $\omega$ is equal to one if the medium is saturated and zero if the medium is unsaturated. The term $S_S(\mathbf{x})$ represents the specific storage, $C(h,\mathbf{x}) = \mathrm{d}\theta(h,\mathbf{x})/\mathrm{d}h$ is the soil moisture capacity, and $K(h,\mathbf{x})$ is the hydraulic conductivity constitutive function. In equation (2), $h_1$ is the prescribed head at $\Gamma_1$, $q$ is the specific flux at $\Gamma_2$, and $h_0$ is the initial pressure head.

[10] We adopted the *Gardner* [1958] model to describe the hydraulic conductivity-pressure head relationship

$$K(h,\mathbf{x}) = K_S(\mathbf{x})\mathrm{e}^{\alpha(\mathbf{x})h}, \qquad (3)$$

where $K_S(\mathbf{x})$ is the saturated conductivity, and $\alpha(\mathbf{x})$ is the pore-size distribution parameter. The corresponding consistent moisture water content relationship developed by *Russo* [1988] was used:

$$\theta(h,\mathbf{x}) = (\theta_S - \theta_r)\left\{e^{0.5\alpha(\mathbf{x})h}[1-0.5\alpha(\mathbf{x})h]\right\}^{2/2+m} + \theta_r. \quad (4)$$

$\theta_S$ and $\theta_r$ are the saturated and residual moisture contents. $m$ is related to the tortuosity of the soil and is assumed to be zero. We chose these models because the spatial variability of parameters in equations (3) and (4) in the field has been well documented [see *Russo and Bouton*, 1992].

[11] In this application, we use the code VSAFT3 (Variably SAturated Flow and Transport 3-D) developed by *Srivastava and Yeh* [1992] to solve equation (1).

### 2.2. Simultaneous Successive Linear Estimator

[12] The following paragraphs discuss the stochastic estimator for interpreting sequential pumping tests in unconfined aquifers. The estimator is built upon the work by *Zhu and Yeh* [2008] and *Zhu et al.* [2011] which is based on successive linear estimator by *Yeh et al.* [1996] and SimSLE by *Xiang et al.* [2009]. Later, the algorithm is formulated for a highly parameterized heterogeneous conceptual model and an equivalent homogeneous conceptual model.

#### 2.2.1. Highly Parameterized Heterogeneous Conceptual Model

[13] This algorithm first conceptualizes the spatially varying natural log of a hydraulic parameter value as a stochastic process in space or a spatial random field:

$$Y_i(\mathbf{x}) = \overline{y_i}(\mathbf{x}) + y_i(\mathbf{x}), \quad (5)$$

where $\overline{y}_i(\mathbf{x})$ is the unconditional mean which could be a function of location $\mathbf{x}$ (i.e., a trend) or a constant, and $y_i(\mathbf{x})$ is the perturbation. The subscript $i$ is the parameter index and ranges from 1 to $N$. In this study $N=4$, when $i=1$, the parameter is $K_S$, when $i=2$, the parameter is $S_S$, when $i=3$, the parameter is $\alpha$, and when $i=4$, the parameter is $\theta_S$. The spatial distribution of each parameter is implicitly assumed to be normal and characterized by its mean, variance, and correlation structure. The use of the natural logarithm of a parameter aims to avoid any negative value for its estimate. This estimation algorithm requires the aquifer to be discretized into $n$ material blocks and $m$ computational finite elements. The vector $\mathbf{x}$ in this paper denotes the location of either a material block or a node of the computational finite element. The discretization of the aquifer for material blocks may not be the same as that for the computational finite element as discussed in section 3. The number of parameter values to be estimated for the entire aquifer is the number of material blocks multiplied by the number of parameters. For example, if $K_S$, $S_S$, $\alpha$, and $\theta_S$ are to be estimated, the total number of parameter values to be estimated will be $4n$. Note that the matrices and vectors are shown in bold characters, and the dimension of each matrix is shown in parentheses.

[14] If necessary conditions for the estimation problem to be well defined [see *Yeh et al.*, 2011; *Mao et al.*, 2013a] are not met, an infinite number of possible values for each parameter exist. For such ill-defined estimation problems, the goal of our algorithm is to seek the most likely, conditional, effective $K_S$, $S_S$, $\alpha$, and $\theta_S$ fields, which will honor the measurements of the parameters (hard data) and the measurements of aquifer responses (such as heads) at sampling locations, and which will provide statistically unbiased predictions of flow fields. Additionally, the algorithm estimates the uncertainty of the conditioned effective parameter fields, which is reflected in the residual variance of each parameter at each material block.

[15] Suppose measurements of parameters $\mathbf{y}_i^*$ $(i=1, N)$ at locations from 1 to $\nu_i$ are available. A stochastic linear estimator (cokriging) can be used to derive a conditional mean parameter field. That is,

$$\mathbf{y}_{ci} = \sum_{i=1}^{N} \boldsymbol{\lambda}_i{}^T \mathbf{y}_i^*, \quad (6)$$

where superscript $T$ denotes transpose, $\mathbf{y}_{ci}(n\times 1)$ is the estimated $i$th hydraulic parameter perturbation of $n$ material blocks over the entire domain, conditioned on the measurements (subscript $c$ denotes conditioned value); $\mathbf{y}_i^*(\nu_i \times 1)$ is the perturbation of the hydraulic parameter measured at the sample locations. $\boldsymbol{\lambda}_i(\nu_i \times n)$ is a weight matrix which can be derived using the following relationship:

$$\begin{bmatrix} \mathbf{R}_{y_1y_1} & \cdots & \mathbf{R}_{y_1y_N} \\ \vdots & \ddots & \vdots \\ \mathbf{R}^T_{y_1y_N} & \cdots & \mathbf{R}_{y_Ny_N} \end{bmatrix} \begin{bmatrix} \boldsymbol{\lambda}_1 \\ \vdots \\ \boldsymbol{\lambda}_N \end{bmatrix} = \begin{bmatrix} \mathbf{R}'_{y_1y_1} \\ \vdots \\ \mathbf{R}'_{y_Ny_N} \end{bmatrix}. \quad (7)$$

$\mathbf{R}_{y_iy_j}(\nu_i \times \nu_j)$ denotes the cross covariance between $y_i$ and $y_j$ at the locations where they are measured. If $i=j$, $\mathbf{R}_{y_iy_i}(\nu_i \times \nu_i)$ becomes the covariance of the $i$th parameter. The diagonal components of $\mathbf{R}_{y_iy_i}$ are the variance of parameter $Y_i$. We used the exponential model for covariance in this study. On the right-hand side of equation (7), $\mathbf{R}'_{y_iy_i}(\nu_i \times n)$ is the covariance between the parameter values at the locations where they are to be estimated and those at locations where we have measurements. Here we assume that the parameters of all material blocks are to be estimated.

[16] After incorporation of hard data into the estimation, the conditional perturbation equation (6) is added to the unconditional mean $\overline{y}_i(\mathbf{x})$ to obtain $\mathbf{Y}^1_{ic}(\mathbf{x})$, where subscript $c$ denotes the conditioned value and superscript 1 indicates the first estimate derived from cokriging using different parameters. Meanwhile, the uncertainty associated with the parameter is updated using a first-order approximation:

$$\boldsymbol{\varepsilon}^1_{y_iy_j}(\mathbf{x}_0,\mathbf{x}_d) = \mathbf{R}_{y_iy_j}(\mathbf{x}_0,\mathbf{x}_d) - \sum_{i=1}^{n}\sum_{l=1}^{\nu_i} \boldsymbol{\lambda}_{il}{}^T(\mathbf{x}_0)\mathbf{R}_{y_iy_l}(\mathbf{x}_l,\mathbf{x}_d), \quad (8)$$

where $\boldsymbol{\varepsilon}^1_{y_iy_j}(\mathbf{x}_0,\mathbf{x}_d)$ represents the residual covariance or cross covariance of the perturbation at location $\mathbf{x}_0$ and $\mathbf{x}_d$ $(d=1, \ldots, n)$. If $i=j$, $\boldsymbol{\varepsilon}^1_{y_iy_i}$ is the residual variance of the parameter at that location, which represents the uncertainty of the estimate at that location. In other words, the value of the residual variance will become zero if an error-free measurement of $Y_i$ is given at that location.

[17] After conditioning the estimates with hard data sets, the estimates are then conditioned with the secondary information, i.e., observed head data from sequential pumping tests, to improve the resolution of the estimates. In order to do so, a linear estimator, based on the difference between the observed and simulated heads at measurement locations using previously estimated parameters, is employed:

$$\mathbf{Y}_{ic}^{r+1} = \mathbf{Y}_{ic}^{r} + \boldsymbol{\chi}_i^r(\mathbf{h}^* - \mathbf{h}^r), \tag{9}$$

where $\mathbf{Y}_{ic}^{r}$, a $n \times 1$ vector, is the estimated value of the $i$th parameter conditioned with either hard or head data sets at iteration $r$ where $r$ is the iteration index. When $r = 1$, $\mathbf{Y}_{ic}^{r=1}$ is the cokriged parameter field conditioned on the hard data. $\mathbf{h}^r(\eta \times 1)$ denotes the corresponding $\eta$ heads simulated with the estimated parameters at iteration $r$. Here $\eta$ is the total number of head observations in time and space from all pumping tests. Further, $\mathbf{h}^*(\eta \times 1)$ is the observed head and $\boldsymbol{\chi}^r(n \times \eta)$ is the weighting coefficient matrix. This matrix is derived by solving the following equation:

$$\boldsymbol{\chi}_i^r \boldsymbol{\varepsilon}_{pp}^r + \pi \mathbf{I} = \boldsymbol{\varepsilon}_{py_i}^r. \tag{10}$$

$\boldsymbol{\varepsilon}_{py_i}$ on the right-hand side of equation (10) represents the residual cross-covariance matrix between the observed heads and the parameters to be estimated, which is derived in equation (12). $\mathbf{I}$ is the identity matrix, and $\pi$ is the stabilizing factor. These two terms are employed to improve the conditional number of equation (10). $\pi$ is determined dynamically according to a specified multiplier and the maximum value of the diagonal terms of $\boldsymbol{\varepsilon}_{pp}^r$ at $r$th iteration.

[18] To derive $\boldsymbol{\varepsilon}_{pp}^r$ and $\boldsymbol{\varepsilon}_{py_i}^r$ used in equation (10), a first-order approximation of head perturbations is used:

$$\mathbf{p} \approx \sum_{i=1}^{N} \mathbf{J}_{py_i} \mathbf{y}_i, \tag{11}$$

where $\mathbf{p}(\eta \times 1)$ is the head perturbation, and $y_i$ is the parameter perturbation. $\mathbf{J}_{py_i}$ is the Jacobian matrix $(\eta \times n)$ for the sensitivity of observed heads with respect to parameter $Y_i$. The sensitivity is evaluated by an adjoint state method (see section 2.3) based on the values of $\mathbf{Y}_{ic}^{r}$ at iteration $r$. The sensitivity is then used to obtain the cross covariance between heads and hydraulic parameters:

$$\boldsymbol{\varepsilon}_{py_i} = \sum_{j=1}^{N} \mathbf{J}_{py_i} \boldsymbol{\varepsilon}_{y_i y_j}. \tag{12}$$

$\boldsymbol{\varepsilon}_{y_i y_i}(n \times n)$ is the updated residual covariance using equation (8) after cokriging or using equation (14) when $r > 1$. Head covariance $\boldsymbol{\varepsilon}_{pp}(\eta \times \eta)$ based on the first-order analysis can be written as

$$\boldsymbol{\varepsilon}_{pp} = \sum_{i=1}^{N} \sum_{j=1}^{N} \mathbf{J}_{py_i} \boldsymbol{\varepsilon}_{y_i y_j} \mathbf{J}_{py_j}^T. \tag{13}$$

The above expression $\boldsymbol{\varepsilon}_{y_i y_j}$ could be cross covariance between parameter $y_i$ and parameter $y_j$ if they are statistically correlated.

[19] After updating the estimate using equation (9), covariance matrix $\boldsymbol{\varepsilon}_{y_i y_j}^r$ at $r$th iteration is subsequently updated to reflect the incorporation of the head data sets from pumping tests. Specifically,

$$\boldsymbol{\varepsilon}_{y_i y_j}^{r+1}(\mathbf{x}_0, \mathbf{x}_d) = \boldsymbol{\varepsilon}_{y_i y_j}^{r}(\mathbf{x}_0, \mathbf{x}_d) - \sum_{l=1}^{\eta} \boldsymbol{\chi}_{il}^r(\mathbf{x}_0) \boldsymbol{\varepsilon}_{y_i p}^r(\mathbf{x}_l, \mathbf{x}_d). \tag{14}$$

Note that equation (9) is a linear estimator and uses head differences to linearly extrapolate the new values of the parameters; however, the relationship between heads and parameters is nonlinear [*Yeh et al.*, 1996]. As a result, equation (9) does not fully exploit the head information from pumping tests. To maximize the information content in heads about parameter values or to fully consider the nonlinear relationship, procedures from equation (9) through equation (14) are iterated until convergence criteria are met. The iteration stops when the change of the largest variance of the estimated parameter field and/or when the change of the maximum head misfit among observation data are/is smaller or equal to a specified value.

### 2.2.2. Equivalent Homogeneous Conceptual Model

[20] The above SimSLE for the highly parameterized heterogeneous conceptual model is also readily capable of estimating effective parameters for an equivalent homogeneous conceptual model. For the homogeneous conceptual model, one only has to estimate four effective parameters ($K_S$, $S_S$, $\alpha$, and $\theta_S$) for the entire aquifer. Each of them is conceptualized as a random variable, instead of a stochastic process. Each random variable represents the uncertainty about the parameter value due to the lack of measurements of this parameter or estimation errors due to errors in measurements of aquifer responses.

[21] The algorithm for the homogeneous conceptual model is the same as that for the heterogeneous model, with the exception that the cokriging procedure that uses measurements of hydraulic parameters is skipped. Note that only one uniform value is sought for each parameter over the entire aquifer, and the errors in parameter value are spatially uncorrelated. Therefore, dimensions of those matrices or vectors are changed accordingly, i.e., $\mathbf{J}_{py_i}(\eta \times 1)$, $\boldsymbol{\varepsilon}_{y_i y_j}(1 \times 1)$, $\mathbf{R}_{py_i}(\eta \times 1)$, $\mathbf{R}_{pp}(\eta \times \eta)$, $\mathbf{R}_{y_i y_j}(1 \times 1)$, and $\boldsymbol{\chi}(\eta \times 1)$.

[22] For this model, the Jacobian matrix or sensitivity is calculated by the perturbation method since the adjoint method offers no advantages under this condition. The objective of this homogeneous SimSLE is to derive an effective value for each parameter. They are then used as prior information for the subsequent SimSLE for heterogeneous conceptual model.

## 2.3. Sensitivity Evaluation by Adjoint State Method

[23] The evaluation of sensitivity for the heterogeneous conceptual model is carried out by the adjoint state method. We briefly discuss this method here, and details of the derivation are referred to *Li and Yeh* [1998, 1999] and *Hughson and Yeh* [2000]. The sensitivity is evaluated at the mean value of each parameter. The subscript $i$ from parameter $Y_i$ is dropped off here for simplification. The marginal sensitivity for a parameter $Y$ of a performance function $G$ is

$$\frac{\partial P}{\partial Y} = \int_T \int_\Omega \left( \frac{\partial G}{\partial Y} + \frac{\partial G}{\partial h} \frac{\partial h}{\partial Y} \right) \mathrm{d}\Omega \mathrm{d}t. \tag{15}$$

[24] The first term inside the integral represents the direct impact of parameter $Y$ on the performance function $G$, and the second term means the indirect impact via pressure head $h$. $T$ and $\Omega$ are the temporal and spatial domains, respectively. In our research, we choose the performance function as

$$G = h\delta(\mathbf{x}-\mathbf{x}_k,\, t-t_c), \tag{16}$$

where $\delta(\mathbf{x}-\mathbf{x}_k, t-t_c)$ is the Kronecker delta function, and the performance function represents the observed head at location $\mathbf{x}_k$ and time $t_c$.

[25] We next differentiate the governing equation (1) with respect to any log hydraulic parameter, multiply the result with an arbitrary function $\Phi$ (adjoint state variable), and rearrange the resultant equation. We have

$$\begin{aligned}
&\int_T \Bigg\{ -\int_\Omega \phi \frac{\partial K(h)}{\partial h} \nabla\Phi\nabla(h+z)\mathrm{d}\Omega - \int_\Omega \frac{\partial K(h)}{\partial Y}\nabla\Phi\nabla(h+z)\mathrm{d}\Omega \\
&+\int_\Omega \phi\nabla\cdot[K(h)\nabla\Phi]\mathrm{d}\Omega - \int_\Omega \frac{\partial[\beta S_S + C(h)]}{\partial Y}\frac{\partial h}{\partial t}\Phi\mathrm{d}\Omega \\
&+\int_\Omega [\beta S_S + C(h)]\frac{\partial \Phi}{\partial t}\phi\mathrm{d}\Omega \Bigg\}\mathrm{d}t \\
&+\int_T \Bigg\{ \int_\Gamma \phi K(h)\nabla\Phi\mathrm{d}\Gamma - \int_\Gamma \Phi K(h)\nabla\phi\mathrm{d}\Gamma + \int_\Gamma \Phi\frac{\partial q}{\partial Y}d\Gamma \Bigg\}\mathrm{d}t \\
&-\int_\Omega [\beta S_S + C(h)]\phi\Phi\Big|_{t=0}^{t=\mathrm{final}}\mathrm{d}\Omega = 0,
\end{aligned} \tag{17}$$

where $\phi = \partial h/\partial Y$ is the sensitivity of pressure with respect to any parameter $Y$. We then add equation (17) to both sides of equation (15) to obtain

$$\begin{aligned}
\frac{\partial P}{\partial Y} =& \int_T\int_\Omega \Bigg\{ \left(\frac{\partial G}{\partial Y}\right) + \phi\Bigg(\frac{\partial G}{\partial h} + \nabla\cdot[K(h)\nabla\Phi] \\
&+[\beta S_S + C(h)]\frac{\partial\Phi}{\partial t} - \frac{\partial K(h)}{\partial h}\nabla\Phi\nabla(h+z)\Bigg)\Bigg\}\mathrm{d}\Omega\mathrm{d}t \\
&+\int_T\int_\Omega \left\{ -\frac{\partial K(h)}{\partial Y}\nabla\Phi\nabla(h+z) - \frac{\partial[\beta S_S + C(h)]}{\partial Y}\frac{\partial h}{\partial t}\Phi \right\}\mathrm{d}\Omega\mathrm{d}t \\
&+\int_T \left( \int_\Gamma \phi K(h)\nabla\Phi\mathrm{d}\Gamma - \int_\Gamma \Phi K(h)\nabla\phi\mathrm{d}\Gamma + \int_\Gamma \Phi\frac{\partial q}{\partial Y}\mathrm{d}\Gamma \right)\mathrm{d}t \\
&-\int_\Omega [\beta S_S + C(h)]\phi\Phi\Big|_{t=0}^{t=\mathrm{final}}\mathrm{d}\Omega.
\end{aligned} \tag{18}$$

In order to eliminate the terms relating to $\phi$ in equation (18), we set the terms inside the large parentheses zero. That is,

$$\begin{aligned}
&\nabla\cdot[K(h)\nabla\Phi] - \frac{\partial K(h)}{\partial h}\nabla\Phi\nabla(h+z) + \delta(\mathbf{x}-\mathbf{x}_k, t-t_c) \\
&= -[\beta S_S + C(h)]\frac{\partial\Phi}{\partial t}.
\end{aligned} \tag{19}$$

Equation (19) is the adjoint state equation, which will be solved for $\Phi$ with the following boundary and final time conditions

$$\begin{aligned}
&\Phi = 0 \text{ at } t = t_{\mathrm{final}} \\
&\Phi = 0 \text{ at } \Gamma_1 \\
&K(h)\nabla\Phi = 0 \text{ at } \Gamma_2.
\end{aligned} \tag{20}$$

Notice that while this adjoint equation is linear, it must be solved once for each head observation time at a given observation location. This is necessary because the hydraulic conductivity and moisture capacity terms in equation (19) vary with the pressure head, which changes with time. Therefore, the use of a large number of temporal head data for estimation would significantly increase computational efforts. It may not improve the estimates since the data may carry redundant information about the heterogeneity [*Mao et al.*, 2013].

[26] With these choices of adjoint state variable, performance function, and boundary conditions, equation (18) becomes

$$\begin{aligned}
\frac{\partial P}{\partial Y} = \frac{\partial h}{\partial Y} = \int_T\int_\Omega \Bigg\{ &-\frac{\partial K(h)}{\partial Y}\nabla\Phi\nabla(h+z) \\
&-\frac{\partial[\beta S_S + C(h)]}{\partial Y}\frac{\partial h}{\partial t}\Phi \Bigg\}\mathrm{d}\Omega\mathrm{d}t.
\end{aligned} \tag{21}$$

[27] This leads to the sensitivity of an observed head at location $\mathbf{x}_k$ and time $t_c$ with respect to each parameter at element $e$:

$$\frac{\partial h(\mathbf{x}_k, t_c)}{\partial \ln K_S(\mathbf{x}_e)} = \int_T\int_{\Omega_e} -K(h)\nabla\Phi\nabla(h+z)\mathrm{d}\Omega\mathrm{d}t, \tag{22}$$

$$\frac{\partial h(\mathbf{x}_k, t_c)}{\partial \ln \alpha(\mathbf{x}_e)} = \int_T\int_{\Omega_e} \left[ -\alpha\frac{\partial K(h)}{\partial \alpha}\nabla\Phi\nabla(h+z) - \alpha\frac{\partial C(h)}{\partial\alpha}\frac{\partial h}{\partial t}\Phi \right]\mathrm{d}\Omega\mathrm{d}t, \tag{23}$$

$$\frac{\partial h(\mathbf{x}_k, t_c)}{\partial \ln S_S(\mathbf{x}_e)} = \int_T\int_{\Omega_e} -S_S\frac{\partial h}{\partial t}\Phi\mathrm{d}\Omega\mathrm{d}t, \tag{24}$$

$$\frac{\partial h(\mathbf{x}_k, t_c)}{\partial \ln \theta_S(\mathbf{x}_e)} = \int_T\int_{\Omega_e} -\theta_S\frac{\partial C(h)}{\partial\theta_S}\frac{\partial h}{\partial t}\Phi\mathrm{d}\Omega\mathrm{d}t. \tag{25}$$

[28] Generally speaking, in the finite element method, the computation grid is commonly set to be the same as the material block (i.e., an element where uniform hydraulic properties are assigned), and therefore, integration domain $\Omega_e$ in the above equations is itself an element. For variably saturated flow system, finer computation grids are needed for the unsaturated region to expedite convergence or ensure the mass balance. Using the same number of elements for materials as the number of computational elements, the computational burden in terms of speed and memory requirements can increase drastically. To alleviate these problems, we developed a dual grid or element system: computational and material grids.

[29] The computational grid is overlaid on the material grid. As a result, the number of material elements where

parameters are to be estimated remains the same, while the computational grids are refined to increase the accuracy of predicted pressure head at location where the hydraulic gradient is high. This permits dynamical change in the computation grid without changing the number of parameters to be estimated. The accuracy of the sensitivity based on equations (22)–(25) is also improved since the integration domain $\Omega_e$ (the material element) contains several computation grids.

### 2.4. Hybrid Computing by MPI and OpenMP

[30] The adjoint state approach calculates sensitivity for each observation data independently, which is suitable for the parallel computing algorithm by Message Passing Interface (MPI) [*Gropp et al*., 1999] on a cluster system. For this work, we also utilized another parallel computing technique, OpenMP [*Chapman et al*., 2007], which takes advantage of multiple cores on each computer. The Algebraic Multigrid Methods for Systems (SAMG) for solving sparse matrix was used here [*Stüben and Clees*, 2010]. Tests using a forward model showed that this new solver accelerated computational speed up to 20 times. During the code execution, MPI is used to distribute the workload to different machines. On each machine, OpenMP is used for solving the groundwater governing equation (1), adjoint state equation (19), and some matrix multiplications, i.e., the calculation of cross covariance in equation (12). A cluster with 6 Dell PowerEdge R410 servers was used for this study. Each server was equipped with two quad-core Intel XeonE5620 2.4 GHz CPUs and 32 GB physical memory.

## 3. Numerical Experiments

### 3.1. Numerical Model Setup

[31] A 3-D synthetic unconfined aquifer was created to test the joint interpretation algorithm. The aquifer was 50 m $\times$ 50 m $\times$ 9 m and was discretized into 11,250 uniform material blocks where each block was 2 m $\times$ 2 m $\times$ 0.5 m in size. The computational finite element grid consisted of 87,856 rectangular cuboid elements of different sizes and 95,220 nodes. A computational grid with vertical space of 0.2 m was assigned near the water table and 0.5 m for the rest of the domain. In the horizontal $x$ direction, the grid space was 0.5 m for the segment from $x = 11$ to 39 m, and 1 m for the elements on both sides of the segment, and became 2 m for the rest till the boundary. The same discretization scheme was used for the $y$ direction.

[32] Hydraulic parameters (ln $K_S$, ln $S_S$, ln $\alpha$, and ln $\theta_S$) of each material block were treated as stochastic processes or random fields with jointly normal distributions. The parameters were assumed to be independent with each other. One realization of each random parameter field was generated by the spectral method [*Gutjahr*, 1989] (see Figure 1).

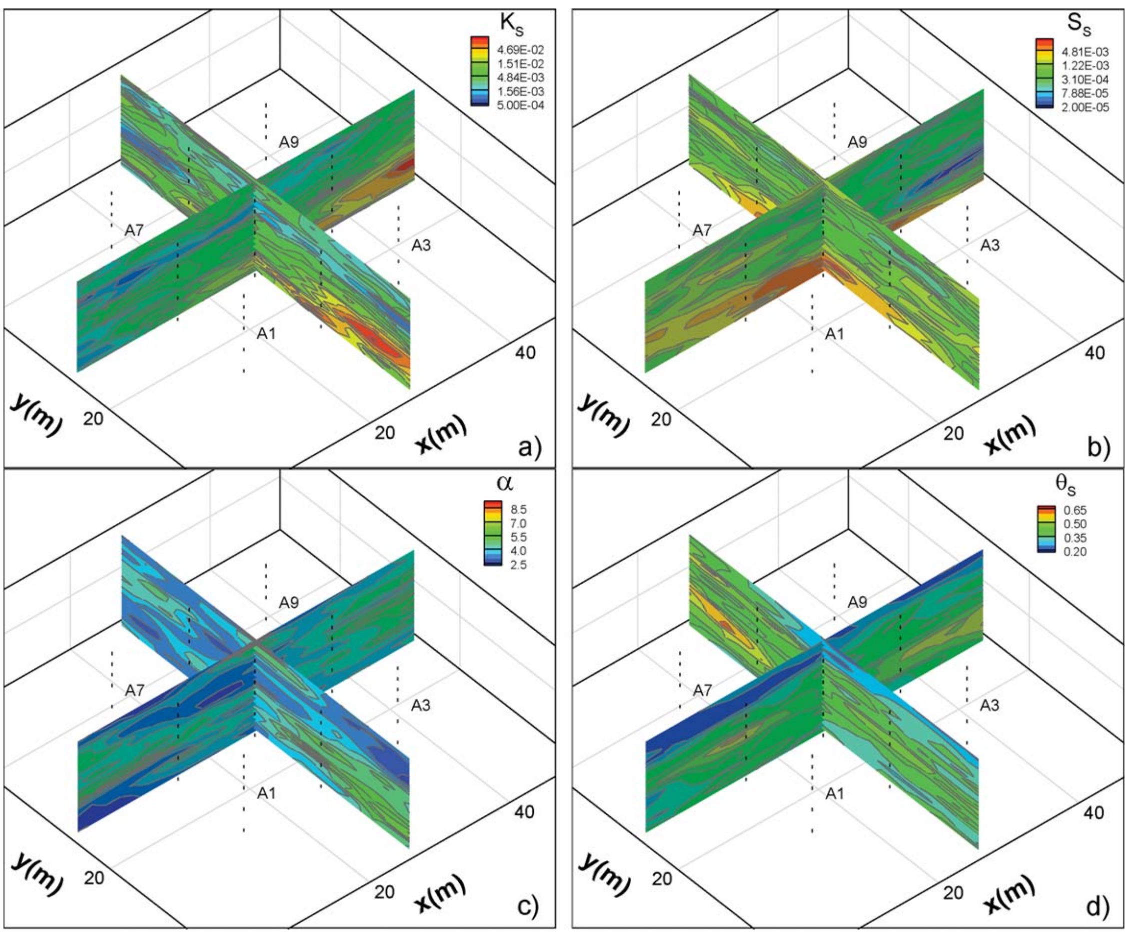


**Figure 1.** Generated true random fields for (a) $K_S$, (b) $S_S$, (c) $\alpha$, and (d) $\theta_S$. The nine columns of points show the location of wells.

**Table 1.** Mean, Variance, and Correlation Scales of the Random Hydraulic Parameters of the 3-D Synthetic Unconfined Aquifer

| | $\ln K_S$ | $\ln S_S$ | $\ln \alpha$ | $\ln \theta_S$ |
|---|---|---|---|---|
| Mean | −5.52 | −7.60 | 2.08 | −0.99 |
| Variance | 1.0 | 1.0 | 0.05 | 0.05 |
| Correlation in $x$ (m) | 30.0 | 30.0 | 30.0 | 30.0 |
| Correlation in $y$ (m) | 30.0 | 30.0 | 30.0 | 30.0 |
| Correlation in $z$ (m) | 2.0 | 2.0 | 2.0 | 2.0 |

The geometric mean of the $K_S$, $S_S$, $\alpha$, and $\theta_S$ is 0.005 m/min, 0.0008/m, 4.0/m, and 0.37. The details of the spatial statistics (mean, variance, and correlation scales) describing the spatial variability of each parameter are listed in Table 1. A correlation scale of 30 m in the horizontal directions and 2 m in the vertical were used to create a layered structure, typical sedimentary environment for a loosely consolidated unconfined aquifer. According to the analysis of field data by *Russo and Bouton* [1992], the variability of unsaturated parameters is usually smaller than that of the $K_S$. The statistics of $S_S$ from previous studies is not readily available. Hence, we assigned it the same correlation scales and variance as those of the $K_S$.

[33] Initial condition was assumed to be hydrostatic with the water table located at $z = 6.7$ m; Constant total head of 6.7 m was assigned to the four sides of the aquifer and no flux boundary on the top and bottom surfaces.

[34] Nine wells were installed in the aquifer (A1–A9 from left to right and then next row, see Figure 1). Three pumping tests were simulated at wells A1, A5, and A9. The screen interval of each pumping well was assumed to be from $z = 0$ to 4 m. During each pumping test, the other eight wells served as observation wells, with point observation at six different levels, $z = 1$, 3, 5, 6, 7, and 8 m across both saturated and unsaturated zones. Each pumping test lasted for 300 min at a discharge of 0.06 $m^3$/min, which is sufficiently long to create a cone of depression covering most of the aquifer domain.

[35] The stopping criteria for the SimSLE are as follows: (1) the largest successive head observation misfit is less than 0.001 m and (2) the largest change of the variance of estimated parameters is smaller than 0.0005. The iteration of the estimation algorithm will stop if one of these two criteria is reached.

[36] *Hughson and Yeh* [2000] suggested that a value ranging from 1 to 4 for the multiplier in $\pi$ (equation (10)) is sufficient for stability. In our SimSLE algorithm, with inclusion of head observations from multiple pumping tests, the head residual covariance $\boldsymbol{\varepsilon}_{pp}$ becomes less diagonally dominant. Equation (10) becomes ill-conditioned, and thus, a larger multiplier is needed to stabilize the equation. In the synthetic case used here, a typical value for the multiplier is 18–25.

### 3.2. Data Selection

[37] According to the cross-correlation analysis by *Mao et al.* [2013], we selected only one to two data points which cover the early and late time periods of each hydrograph for the joint interpretation. Specifically, before the joint interpretation, well hydrographs from all pumping tests were examined. If a complete S-shaped drawdown curve was observed, two data at early time and another two data at late time were sampled. When only part of the S-shaped drawdown curve was observed, usually at wells far away from the pumping well, due to insignificant drawdown at early time, one or two drawdown data at late time were used for analysis. The drawdown data around the intermediate period or the flat part of the S-shaped drawdown curve were not used since the late time information is sufficient for the estimation of unsaturated parameters. A total of 373 head observations were used during inversion for the three pumping tests, including 309 data in the saturated zone and 64 in the unsaturated zone. In addition, the experiments assumed that no measurements of parameters were available.

[38] The robustness of the SimSLE with data infested with noise for flow in saturated aquifers has been demonstrated and discussed by *Xiang et al.* [2009] as well as numerous applications to a large number of sandbox and field experiments mentioned in section 1. All data here were assumed to be error-free to test the validity of the algorithm.

[39] *Bohling and Butler* [2010] advocated that some drawdown data obtained from a sequential pumping test in confined aquifers may contain redundant information and should be excluded from HT analysis due to the principle of reciprocity [*Bruggeman*, 1972]. However, as pointed out by *Huang et al.* [2011], using "redundant" field data in the SimSLE improved the estimates due to issues related to measurement errors. In addition, *Mao et al.* [2013] showed that the principle of reciprocity does not hold in variably saturated flow due to the existence of an advection term. Because of these facts, we utilize all the data, including the pairs which may be redundant.

### 3.3. Performance Criteria

[40] The average absolute error $L_1$ and mean-square error $L_2$ are used as the criteria to evaluate the estimated parameter fields:

$$L_1 = \frac{1}{n}\sum_{i=1}^{n} |\hat{P}_i - P_i|, \quad L_2 = \frac{1}{n}\sum_{i=1}^{n} \left(\hat{P}_i - P_i\right)^2, \tag{26}$$

where $\hat{P}_i$ and $P_i$ represent the true and estimated parameter fields, respectively. We also utilize the correlation coefficient and a scatterplot to describe the fitting between the true and estimated fields. A correlation coefficient close to 1 indicates that the two fields have similar patterns:

$$\mathrm{cor} = \frac{1}{n-1}\frac{\sum_{i=1}^{n}\left(\hat{P}_i - \overline{\hat{P}}\right)\left(P_i - \overline{P}\right)}{\sigma_{\hat{P}_i}\sigma_{P_i}}. \tag{27}$$

$\overline{\hat{P}}$ and $\overline{P}$ are the mean values for two different fields. $\sigma_{\hat{P}_i}$ and $\sigma_{P_i}$ are the standard deviations for each parameter.

[41] These three criteria are also used to evaluate the predicted heads based on the estimated parameter fields during the validation stage (section 4.4).

## 4. Results and Discussion

### 4.1. Equivalent Homogenous Conceptual Model

[42] The purpose of applying SimSLE to the equivalent homogeneous conceptual model is twofold. First, we want

to demonstrate that if necessary conditions are met, there exists a unique solution to the inverse modeling of pumping tests in unconfined aquifers. Second, we want to determine values of effective parameters of the equivalent homogeneous conceptual model, which will be used as starting values for the heterogeneous conceptual model in sections 4.2 and 4.3.

[43] According to *Yeh et al*. [2011], the nonuniqueness issue associated with parameter estimation or inverse problems arises from a lack of information required to make the problems well defined. *Mao et al*. [2013a] suggested that the necessary conditions for a unique estimate of hydraulic parameters of a homogeneous geologic medium under transient variably saturated flow condition are (1) a sufficient number of spatial or temporal head observations; the number of observations depends on the number of unknown parameters; (2) flux boundary condition or discharge of the pumping well; (3) head values covering both saturated and unsaturated conditions; (4) specification of the mathematical model for $K(h,\mathbf{x})$ and $\theta(h,\mathbf{x})$ relationships; and (5) specification of $\theta_r$ or water content data for the estimation of $\theta_S$.

[44] *Mao et al*. [2013a] also demonstrated using 1-D numerical experiments that once these conditions are met and if head and flux measurements are free of errors, the estimates converge to the true values regardless of initial guess values. Under situations where the measurements are infested with noise, the estimates are unique but converge to values that may be different from true values. The discrepancies between the true and estimated values diminish as the number of heads in time and space increases.

[45] In our example, four parameters, $K_S$, $S_S$, $\alpha$, and $\theta_S$, of the 3-D equivalent homogeneous model need to be estimated. 373 head data from both saturated and unsaturated zones from all pumping tests were used. Therefore, the necessary conditions discussed above are met. To show that the unique solution exists, three different guessed values were tried. They all converged to the same values as shown in Figure 2, indicative of the existence of a unique solution. The estimated $K_S = 7.1 \times 10^{-3}$ m/min and $S_S = 9.2 \times 10^{-4}$/m are slightly bigger than the geometric means which are $K_S = 5.0 \times 10^{-3}$ m/min, $S_S = 8.0 \times 10^{-4}$/m. This result is consistent with results of the theoretical analysis of effective parameters by *Yeh et al*. [1985a, 1985b, 1985c]. The estimated effective unsaturated parameters, $\alpha = 3.52$/m and $\theta_S = 0.40$, express the average performance of the unsaturated zone, which merely related to the upper unsaturated part of the aquifer.

### 4.2. Highly Parameterized Heterogeneous Conceptual Model (Case 1)

[46] In this case, we estimated the four hydraulic parameters at each of the 11,250 material blocks of the aquifer. SimSLE requires input of the mean value, correlation scales, and spatial variance of each parameter. For this case and case 2 in section 4.3, we used the effective parameter values obtained from the equivalent homogeneous model as the means, and true values in Table 1 were used for the other inputs. As reported in numerous studies of HT over the past decades [e.g., *Yeh and Liu*, 2000], accuracy of the input spatial statistics (i.e., mean, correlation scale, and the spatial variance) does not significantly impact the results of the stochastic estimator because of the large number of drawdown data sets used in the analysis.

[47] The 3-D cross-sectional views of the estimated parameter fields are shown in Figure 3, while the scatterplots of the true versus estimated parameter values and associated performance criteria are shown in Figure 4. Figure 5 shows

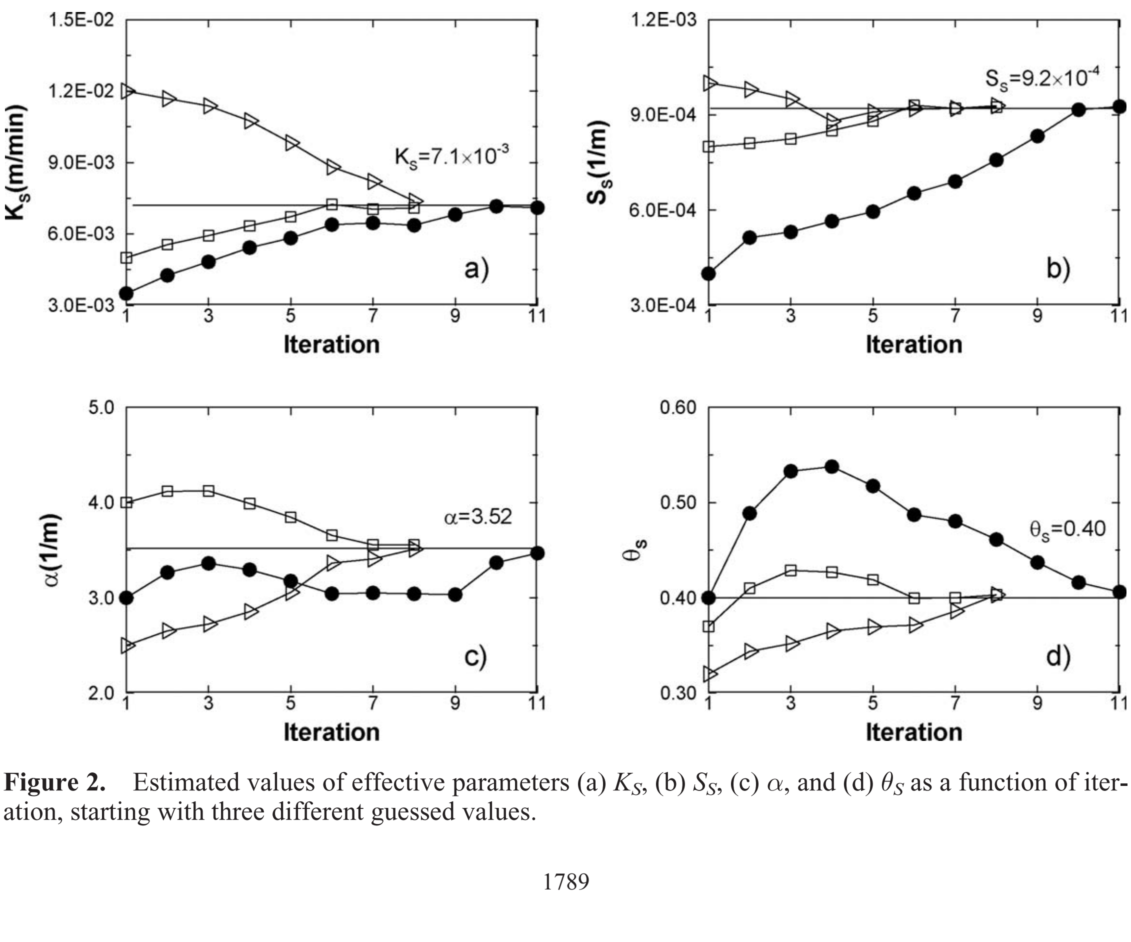


**Figure 2.** Estimated values of effective parameters (a) $K_S$, (b) $S_S$, (c) $\alpha$, and (d) $\theta_S$ as a function of iteration, starting with three different guessed values.

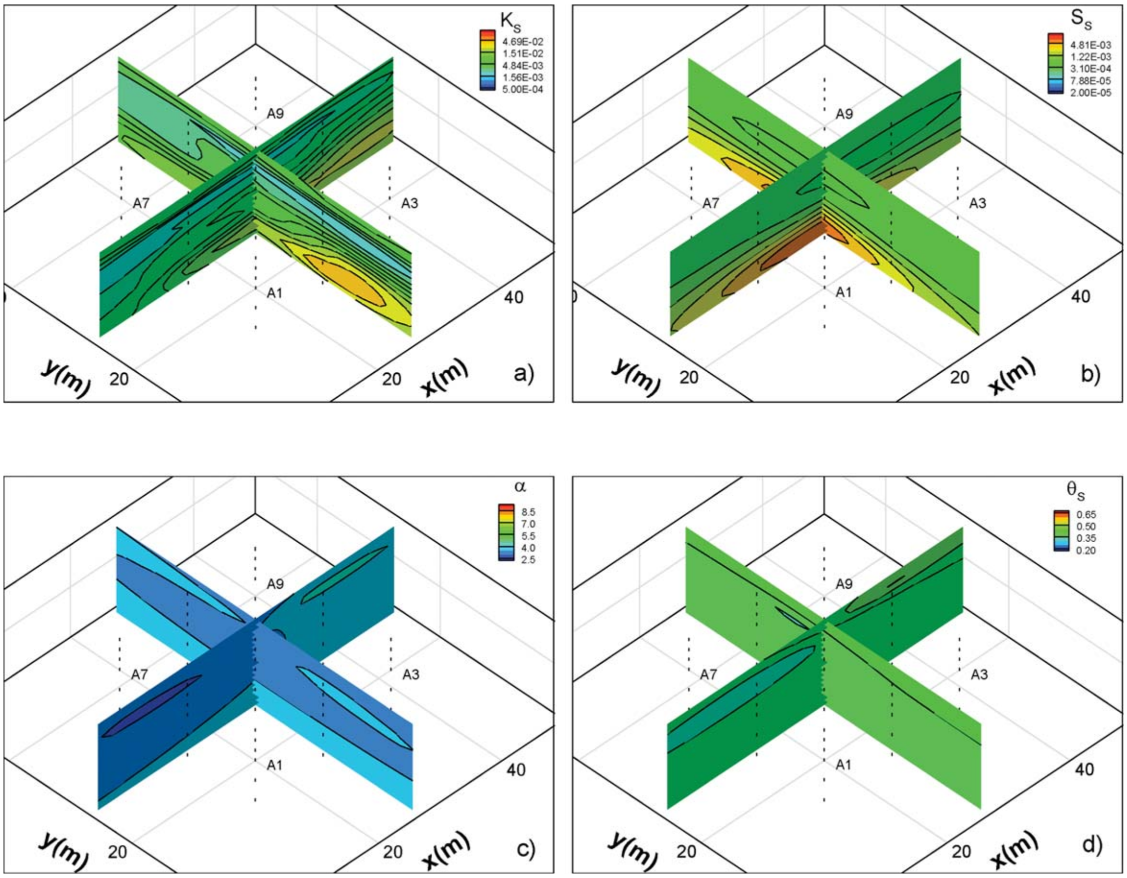


**Figure 3.** Estimated distributions of (a) $K_S$, (b) $S_S$, (c) $\alpha$, and (d) $\theta_S$. The locations for the two cross sections are set exactly the same as those for the true parameters in Figure 1 for comparison purpose.

the spatial variances of the estimated parameter fields as a function of iteration. The residual variance of the estimated parameter fields is shown in Figure 6.

[48] A comparison of the estimated fields (Figure 3) with true fields (Figure 1) reveals that although the two fields are not identical, estimated $K_S$ and $S_S$ fields capture the pattern of the true fields quite well. Specifically, the high $K_S$ zones in the southeast corner and in the northeast corner of the saturated zone are closely depicted by the estimated field. The high $S_S$ zone near the center of the true field below the water table is also captured vividly by the joint interpretation of the sequential pumping tests. Comparing the estimated $\alpha$ and $\theta_S$ fields in Figures 3c and 3d to the true fields in Figures 1c and 1d, we see that the effects of head conditioning are mostly limited to the unsaturated zone.

[49] The robustness of the estimates is also evident if we examine the scatterplots (Figures 4a and 4b). Blue data points in Figures 4a and 4b present scatterplots of the estimated versus true $K_S$ field and those for $S_S$ fields in the saturated zone (0–6.7 m), respectively. On the other hand, the red dots in Figures 4a and 4b represent the corresponding fields in the unsaturated zone (6.7–9.0 m). Based on the plots as well as the performance criteria, estimates of both parameter fields are unbiased with some dispersion since the necessary conditions as discussed in section 4.1 are not met. Nevertheless, the $K_S$ estimates over the entire saturated and unsaturated zone are better than those of $S_S$. It is also apparent that estimated parameters in the saturated zone are closer to the true values than those in the unsaturated zone. The red disk-shaped zone in Figure 4b indicates that the joint interpretation cannot resolve the detailed spatial distribution of $S_S$ values in the unsaturated zone, except the mean value. The scatterplots of $\alpha$ and $\theta_S$ fields in Figures 4c and 4d, respectively, show that the estimated $\alpha$ and $\theta_S$ values in the saturated zone are not possible because they have no influence on the flow in the saturated zone (see equation (1)).

[50] Figure 5 shows that the spatial variances of the estimated $K_S$ and $S_S$ fields increase as iteration progresses to include the nonlinear relationship between parameters and head. This increase indicates that more detailed heterogeneity is revealed. However, the estimated fields remain smoother than the true fields as reflected by their asymptotic values, which are smaller than their true variances. These results are expected since the SimSLE seeks the conditional effective parameters with sparsely distributed monitoring points of the pumping tests [*Yeh et al.*, 1996]. The variances of the estimated unsaturated parameters $\alpha$ and $\theta_S$ are substantially smaller than the true value 0.05, suggesting much smoother estimates for the unsaturated zone. The joint interpretation noticeably yields more detailed information about $\theta_S$ than $\alpha$. These findings are also consistent with the results of the cross-correlation analysis by *Mao et al*. [2013].

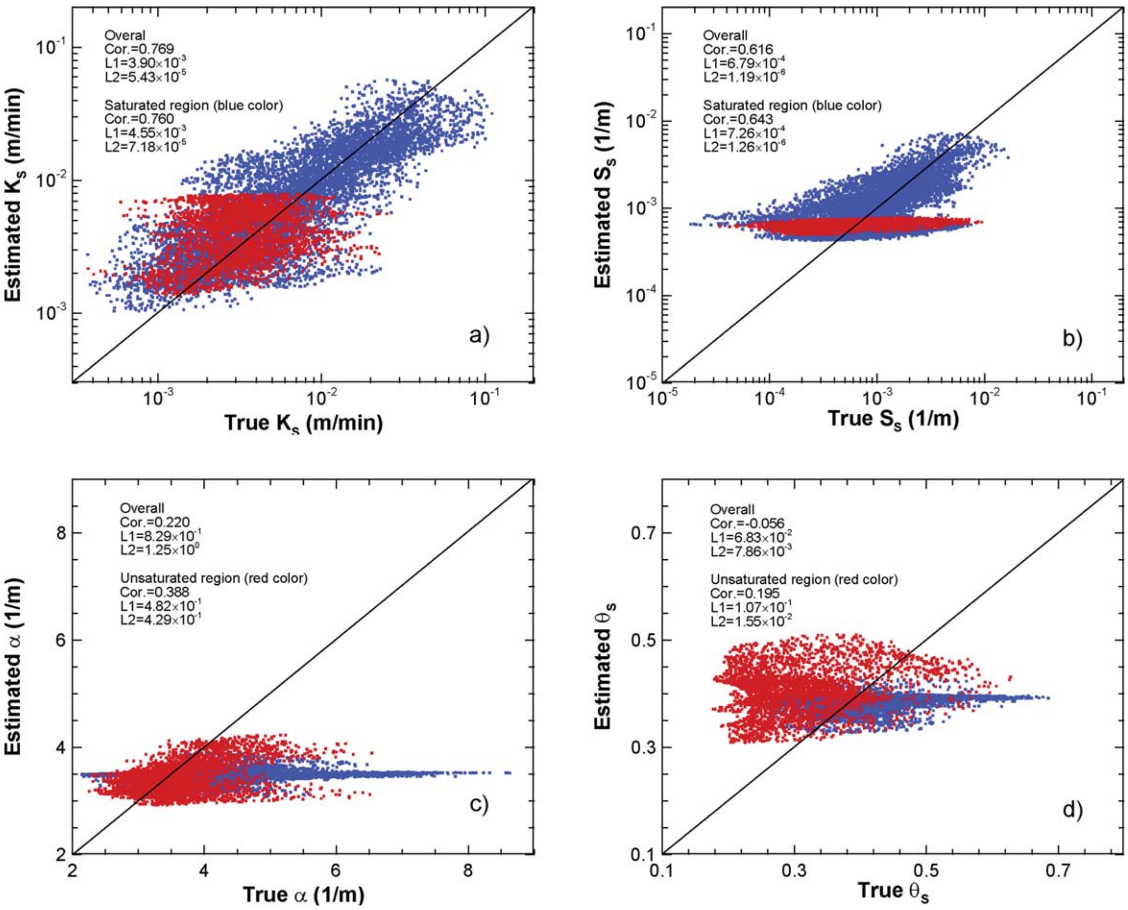


**Figure 4.** Scatterplots of the estimated versus the true for parameters (a) $K_S$, (b) $S_S$, (c) $\alpha$, and (d) $\theta_S$. The red color dots denote those in the unsaturated part of the aquifer (6.7–9.0 m), and the blue dots denote those in the saturated part (0–6.7 m).

[51] The uncertainty associated with the estimate of each parameter is illustrated in Figure 6 as the residual variance. The overall low uncertainty of the $K_S$ estimates over the entire aquifer suggests that the estimates in both saturated and unsaturated zones are closer to the true fields. As expected, large residual variance of $S_S$ remains in the vadose zone, and large residual variances of $\alpha$ and $\theta_S$ stay in the saturated zone.

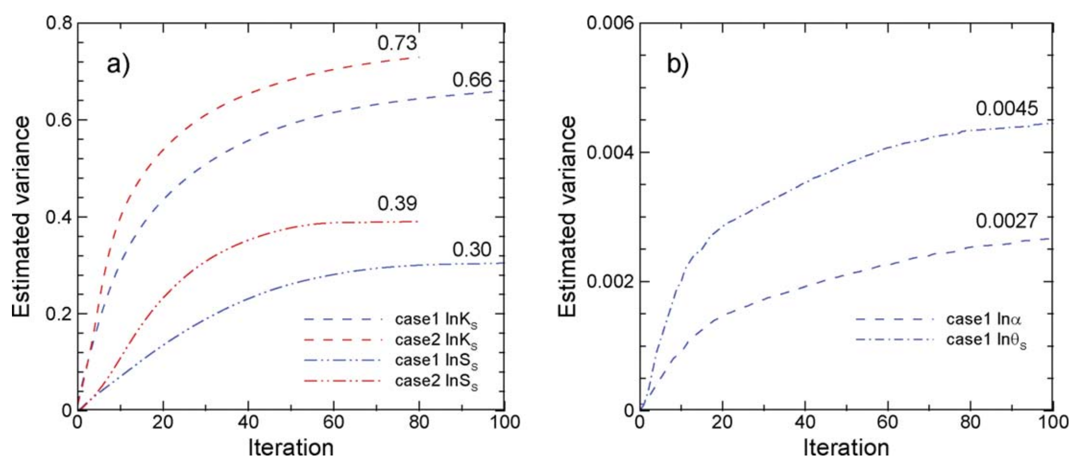


**Figure 5.** Variances of the estimated parameter fields as a function of iteration. Blue lines are for case 1, and red lines are for case 2. The numerical number above each line is the variance value of the final estimate for each parameter.

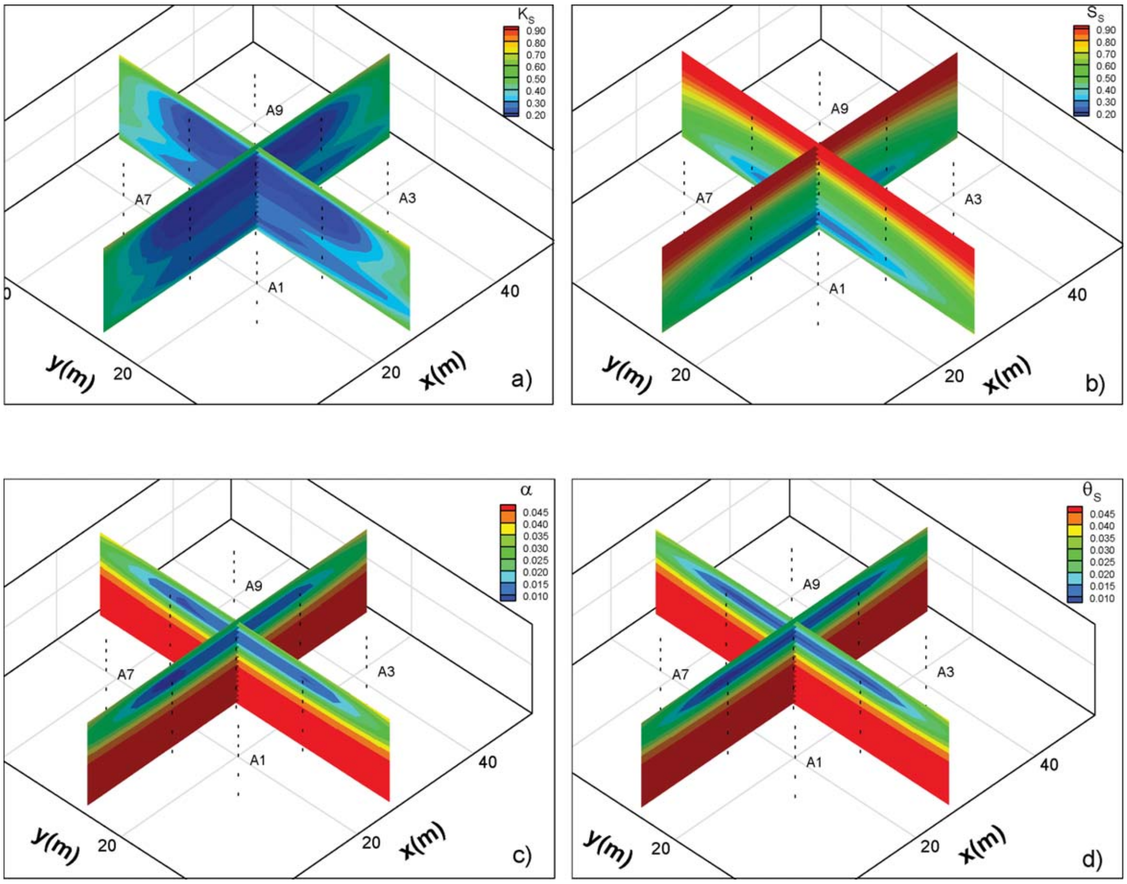


**Figure 6.** Distributions of residual variance for (a) $K_S$, (b) $S_S$, (c) $\alpha$, and (d) $\theta_S$.

### 4.3. Highly Parameterized Heterogeneous Conceptual Model (Case 2)

[52] As discussed by *Mao et al*. [2011] and demonstrated in sandbox experiments by *Berg and Illman* [2012], impacts of variability of unsaturated parameters on the observed heads in saturated zone are insignificant. In this case, we tested this hypothesis by estimating only spatial distributions of $K_S$ and $S_S$ of the entire aquifer while keeping the effective mean values, $\alpha = 3.52$/m and $\theta_S = 0.40$, and ignoring their variability during the joint interpretation.

[53] Figure 7 shows the estimated contour maps for $K_S$ and $S_S$ fields, and Figure 8 shows their scatterplots. Generally, the estimated fields are very similar to these in Case 1. The correlation coefficients are nearly the same for $K_S$: 0.765 for Case 2 and 0.769 for Case 1. For $S_S$, it is lightly smaller in Case 2 (0.579) compared with 0.643 in Case 1. The residual variances of these estimated fields are nearly the same as those in Figures 5a and 5b, and therefore, they are not shown.

[54] However, the spatial variances of estimated fields are larger than the ones in Case 1, 0.73 and 0.39 compared with 0.68 and 0.30 for ln $K_S$ and ln $S_S$, as indicated in Figure 5a. This can be attributed to the assumption that the unsaturated parameters were spatially uniform, and their values were known. The interpretation algorithm, therefore, attempts to adjust the remaining two parameters $K_S$ and $S_S$ to fit head observations. Nevertheless, the impact from unsaturated parameters is insignificant, and the variances of the two parameters increase only slightly.

### 4.4. Validation Through Independent Pumping Tests

[55] Next, we validate the estimated parameter fields by testing their ability to predict drawdowns during an independent pumping test. The cross-correlation analysis by *Mao et al*. [2013] indicated that heads observed at the same observation wells would behave differently if the location of the pumping well is changed since they could be influenced by the heterogeneity near the new pumping well. Therefore, drawdowns due to pumping at well A3 with a screen interval at $z = 0$–4.0 m were used for validating estimated parameters from Case 1 and Case 2.

[56] A homogeneous model which considers anisotropy of the saturated hydraulic conductivity was also employed for the validation (Case 3). The parameters of this homogenous anisotropic field were obtained with SimSLE method which includes anisotropy of hydraulic conductivity in the horizontal and vertical direction ($K_x = K_y$ and $K_z$). With the same data sets used in section 4.1, the estimated effective parameters are $K_x = K_y = 8.54 \times 10^{-3}$ m/min, $K_z = 6.38 \times 10^{-3}$ m/min, $S_S = 1.29 \times 10^{-3}$/m, $\alpha = 3.33$/m, and $\theta_S = 0.42$.

[57] Figures 9a and 9d show the validation results for Case 1 at early time ($t = 10$ min) and late time ($t = 300$ min), respectively. Each figure is a scatterplot of the true total head versus the predicted total head at every node of

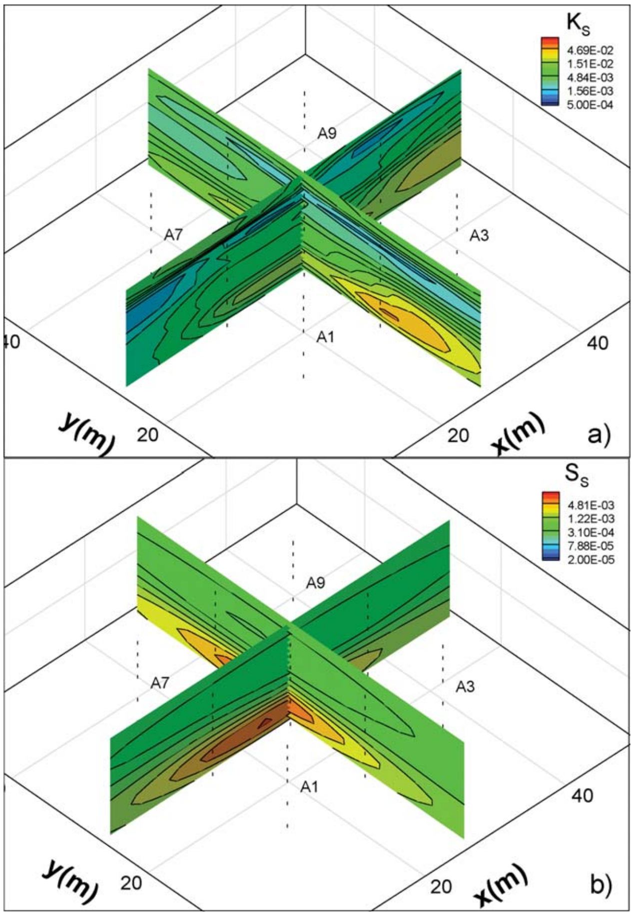


**Figure 7.** Estimated distributions of (a) $K_S$ and (b) $S_S$ with known effective $\alpha$ and $\theta_S$.

the entire domain (i.e., both unsaturated and saturated zones). The performance criteria ($L_1$, $L_2$, and correlation coefficient) are also presented in each figure. Similar plots of the validation results for Case 2 are shown in Figures 9b and 9e and for Case 3 in Figures 9c and 9f.

[58] According to Figures 9a–f and the performance metrics, the prediction based on the estimated parameters from Case 1 and Case 2 are the best. It is hard to distinguish between the results from these two cases, indicative of minor impacts of spatial variability of the unsaturated parameters. As expected, the prediction based on the parameters for an equivalent homogeneous medium is biased and unsatisfactory. The predicted drawdowns are consistently lower than the true drawdowns. This implies that the effective parameters estimated from all the data sets from the pumping tests conducted at A1, A5, and A9 are not the same as the effective parameters for the pumping test conducted at A3. In other words, the effective parameters for the equivalent homogeneous medium are scenario dependent (varying with the geology near the pumping well) as observed and discussed by *Straface et al*. [2007], *Wen et al*. [2010], *Huang et al*. [2011], and R. Sun et al. (A temporal sampling strategy for transient hydraulic tomography analysis, submitted to *Water Resources Research*, 2012, hereinafter referred to as Sun et al., submitted manuscript, 2012) for pumping tests in confined aquifers. The complex spatial distribution of the parameter cross correlation with the head in the unconfined aquifers presented in the study by *Mao et al*. [2013] further elucidates such a scenario-dependent nature of the effective properties. Again, these results reinforce the importance of joint interpretation of sequential pumping tests in unconfined aquifers, and they question the representativeness of those estimates based on models that assume aquifer homogeneity.

## 4.5. Effects of Boundaries

[59] Applications of the HT algorithm to real-world aquifers will likely encounter effects of geologic boundaries. While an investigation of their effects is beyond the scope of this study, we may discuss the effects based on the study of by Sun et al. (submitted manuscript, 2012). In the joint analysis of sequential pumping tests in 2-D depth-averaged confined aquifers, they showed that if boundaries of no flux in the true model were replaced with constant head boundaries, the impermeable boundaries were identified as low conductivity zones near locations of the boundaries. The estimated transmissivity and storage coefficients in other areas of the aquifers remain the same as those based on the correct boundary conditions. That is, effects of impermeable boundaries are

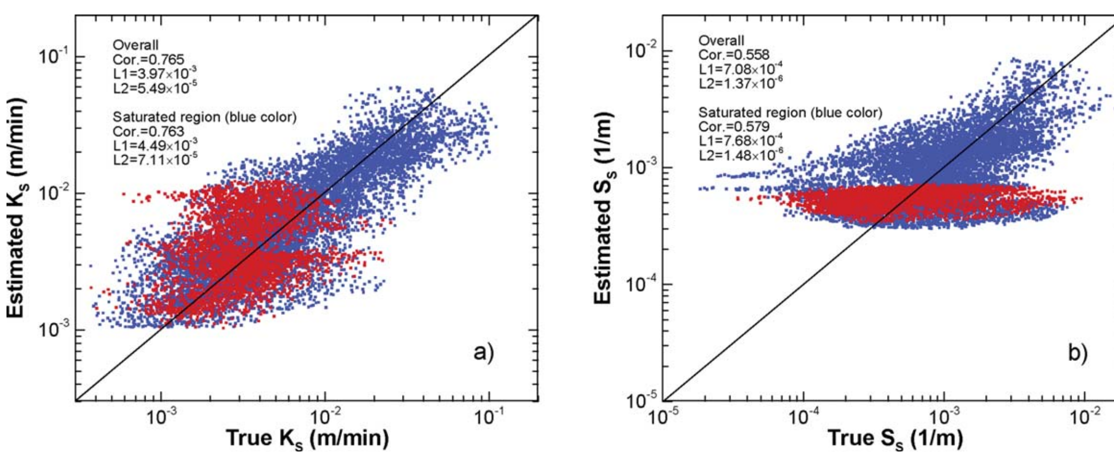


**Figure 8.** Scatterplots of the true versus estimated parameters (a) $K_S$ and (b) $S_S$ with known effective $\alpha$ and $\theta_S$. The red dots are the results for unsaturated part of the aquifer (6.7–9.0 m), and the blue dots are the results for the saturated part (0–6.7 m).

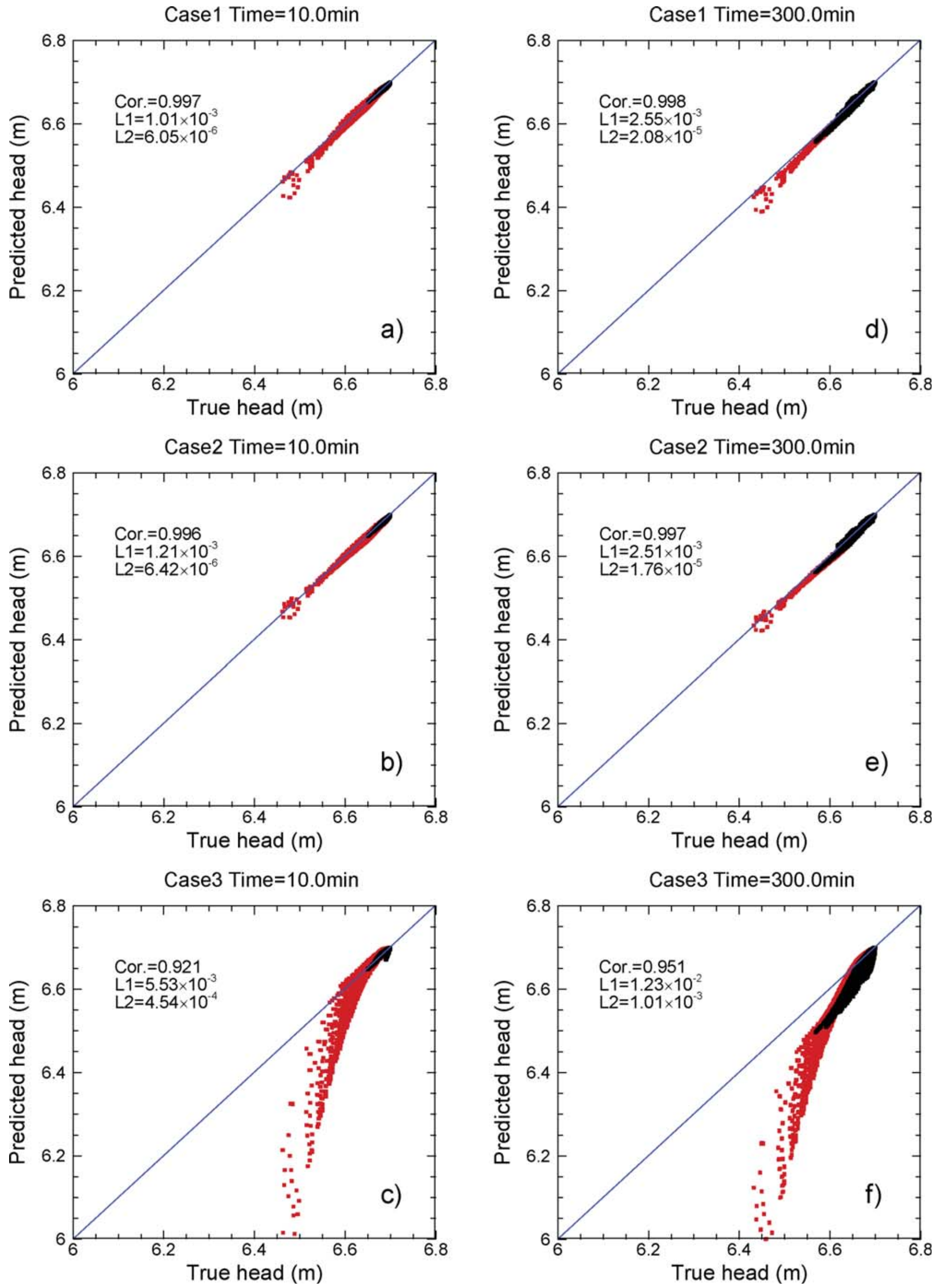


**Figure 9.** Scatterplots of the true versus the predicted total head at every node at early time $t = 10$ min based on the estimated parameters from (a) Case 1, (b) Case 2, and (c) Case 3. The corresponding plots for late time $t = 300$ min are shown in (d)–(f). The black and red dots in each figure are the locations in unsaturated and saturated zones, respectively.

reflected in the head data, and the HT analysis based on SimSLE can decipher them correctly. We believe this finding holds for unconfined aquifers as well.

## 5. Conclusion

[60] In this study, we extended the SimSLE algorithm to HT in variably saturated unconfined aquifers and then tested the algorithm using numerical experiments. Results of the experiments confirm the results of the cross-correlation analysis between heads and aquifer heterogeneity during pumping in unconfined aquifers by *Mao et al*. [2013]. That is, while heterogeneity everywhere within the cone of depression influences head observations at a location during a pumping test, heterogeneity near the observation and the pumping locations has the greatest impacts. As a result, changing the pumping or the observation location yields nonredundant information about heterogeneity of the aquifer. Joint interpretation of a sequential pumping test or a multiwell interference test can thus lead to a high-resolution unconfined aquifer characterization.

[61] We show that the joint interpretation of the sequential pumping tests is capable of identifying the spatial distribution of $K_S$ in both saturated and unsaturated zones, the distribution of $S_S$ in the saturated zone, and the spatial patterns of $\alpha$ and $\theta_S$ in the vadose zone. More importantly, these estimated parameters yield an excellent prediction of temporal and spatial drawdown distributions created by an independent pumping test. On the other hand, the estimated effective parameters for the equivalent homogeneous model of the conventional aquifer analysis yield biased and unsatisfactory prediction of the drawdowns.

[62] Lastly, effects of the spatial variability of the unsaturated parameters on the identification of $K_S$ and $S_S$ are found to be insignificant. Therefore, general knowledge of mean values of $\alpha$ and $\theta_S$ for the entire aquifer is quite sufficient for the estimation of the spatial variability of $K_S$ and $S_S$ in the saturated zone.

[63] **Acknowledgments.** This research was supported through a grant from NSF EAR-1014594 and DoD ESTCP award through a subcontract from AMEC. The first author acknowledges the support of "China Scholarship Council." Support from outstanding scientist award from Department of Education of China to T.-C.J.Y. through Jilin University, China, is also acknowledged.

## References

Berg, S. J., and W. A. Illman (2011a), Capturing aquifer heterogeneity: Comparison of approaches through controlled sandbox experiments, *Water Resour. Res.*, *47*(9), W09514, doi:10.1029/2011WR010429.

Berg, S. J., and W. A. Illman (2011b), Three-dimensional transient hydraulic tomography in a highly heterogeneous glaciofluvial aquifer-aquitard system, *Water Resour. Res.*, *47*, W10507, doi:10.1029/2011WR010616.

Berg, S. J., and W. A. Illman (2012), Improved predictions of saturated and unsaturated zone drawdowns in a heterogeneous unconfined aquifer via transient hydraulic tomography: Laboratory sandbox experiments, *J. Hydrol.*, *470–471*, 172–183, doi:10.1016/j.jhydrol.2012.08.044.

Bohling, G. C., and J. J. Butler (2010), Inherent limitations of hydraulic tomography, *Ground Water*, *48*(6), 809–824, doi:10.1111/j.1745–6584.2010.00757.x.

Bohling, G. C., X. Zhan, J. J. Butler Jr., and L. Zheng (2002), Steady shape analysis of tomographic pumping tests for characterization of aquifer heterogeneities, *Water Resour. Res.*, *38*(12), 1324, doi:10.1029/2001WR001176.

Bohling, G. C., J. J. Butler Jr., X. Zhan, and M. D. Knoll (2007), A field assessment of the value of steady shape hydraulic tomography for characterization of aquifer heterogeneities, *Water Resour. Res.*, *43*(5), W05430, doi:10.1029/2006WR004932.

Boulton, N. S. (1963), Analysis of data from non-equilibrium pumping tests allowing for delayed yield from storage, paper presented at ICE Proceedings.

Brauchler, R., R. Liedl, and P. Dietrich (2003), A travel time based hydraulic tomographic approach, *Water Resour. Res.*, *39*(12), 1370, doi:10.1029/2003WR002262.

Brauchler, R., R. Hu, P. Dietrich, and M. Sauter (2011), A field assessment of high-resolution aquifer characterization based on hydraulic travel time and hydraulic attenuation tomography, *Water Resour. Res.*, *47*(3), W03503, doi:10.1029/2010WR009635.

Bruggeman, G. (1972), The reciprocity principle in flow through heterogeneous porous media, in *Fundamentals of Transport Phenomena in Porous Media*, edited by IAHR, pp. 136–149, Elsevier, Amsterdam.

Brutsaert, W. (1970), Immiscible multiphase flow in ground water hydrology: A computer analysis of the well flow problem, Ph.D. thesis, 119 pp., Colo. State Univ., Fort Collins, Colo.

Cardiff, M., and W. Barrash (2011), 3-D transient hydraulic tomography in unconfined aquifers with fast drainage response, *Water Resour. Res.*, *47*, W12518, doi:10.1029/2010WR010367.

Cardiff, M., W. Barrash, P. K. Kitanidis, B. Malama, A. Revil, S. Straface, and E. Rizzo (2009), A potential-based inversion of unconfined steady-state hydraulic tomography, *Ground Water*, *47*(2), 259–270, doi:10.1111/j.1745–6584.2008.00541.x.

Castagna, M., and A. Bellin (2009), A Bayesian approach for inversion of hydraulic tomographic data, *Water Resour. Res.*, *45*, W04410, doi:10.1029/2008WR007078.

Chapman, B., G. Jost, R. van der Pas, and D. J. Kuck (2007), *Using OpenMP: Portable Shared Memory Parallel Programming*, MIT Press, Cambridge, Mass.

Cooper, H. H., and C. E. Jacob (1946), A generalized graphical method for evaluating formation constants and summarizing well field history, *Am. Geophys. Union Trans.*, *27*, 526–534.

Dagan, G. (1967), A method of determining the permeability and effective porosity of unconfined anisotropic aquifers, *Water Resour. Res.*, *3*(4), 1059–1071, doi:10.1029/WR003i004p01059.

Endres, A., J. Jones, and E. Bertrand (2007), Pumping-induced vadose zone drainage and storage in an unconfined aquifer: A comparison of analytical model predictions and field measurements, *J. Hydrol.*, *335*(1–2), 207–218, doi:10.1016/j.jhydrol.2006.07.018.

Fienen, M. N., T. Clemo, and P. K. Kitanidis (2008), An interactive Bayesian geostatistical inverse protocol for hydraulic tomography, *Water Resour. Res.*, *44*, W00B01, doi:10.1029/2007WR006730.

Gardner, W. (1958), Some steady-state solutions of the unsaturated moisture flow equation with application to evaporation from a water table, *Soil Sci*, *85*(4), 228–232.

Gottlieb, J., and P. Dietrich (1995), Identification of the permeability distribution in soil by hydraulic tomography, *Inverse Probl.*, *11*(2), 353–360.

Gropp, W., E. Lusk, and A. Skjellum (1999), *Using MPI: Portable Parallel Programming with the Message Passing Interface*, 2nd ed., MIT Press, Cambridge, Mass.

Gutjahr, A. L. (1989), *Fast Fourier Transforms for Random Field Generation: Project Report for Los Alamos Grant to New Mexico Tech*, N. M. Inst. of Min. and Technol., Socorro.

Huang, S.-Y., J.-C. Wen, T.-C. J. Yeh, W. Lu, H.-L. Juan, C.-M. Tseng, J.-H. Lee, and K.-C. Chang (2011), Robustness of joint interpretation of sequential pumping tests: Numerical and field experiments, *Water Resour. Res.*, *47*, W10530, doi:10.1029/2011WR010698.

Hughson, D. L., and T.-C. J. Yeh (2000), An inverse model for three-dimensional flow in variably saturated porous media, *Water Resour. Res.*, *36*(4), 829–839, doi:10.1029/2000WR900001.

Illman, W. A., X. Y. Liu, and A. Craig (2007), Steady-state hydraulic tomography in a laboratory aquifer with deterministic heterogeneity: Multi-method and multiscale validation of hydraulic conductivity tomograms, *J. Hydrol.*, *341*(3–4), 222–234, doi:10.1016/j.jhydrol.2007.05.011.

Illman, W. A., A. J. Craig, and X. Liu (2008), Practical issues in imaging hydraulic conductivity through hydraulic tomography, *Ground Water*, *46*(1), 120–132, doi:10.1111/j.1745–6584.2007.00374.x.

Illman, W. A., X. Liu, S. Takeuchi, T.-C. J. Yeh, K. Ando, and H. Saegusa (2009), Hydraulic tomography in fractured granite: Mizunami Underground Research site, Japan, *Water Resour. Res.*, *45*(1), W01406, doi:10.1029/2007WR006715.

Illman, W. A., J. F. Zhu, A. J. Craig, and D. T. Yin (2010), Comparison of aquifer characterization approaches through steady state groundwater model validation: A controlled laboratory sandbox study, *Water Resour. Res.*, *46*, W04502, doi:10.1029/2009WR007745.

Illman, W. A., S. J. Berg, and T.-C. J. Yeh (2012), Comparison of approaches for predicting solute transport: sandbox experiments, *Ground Water*, *50*(3), 421–431, doi:10.1111/j.1745–6584.2011.00859.x.

Lakshminarayana, V., and S. P. Rajagopalan (1978), Type-curve analysis of time-draw down data for partially penetrating wells in unconfined anisotropic aquifers, *Ground Water*, *16*(5), 328–333, doi:10.1111/j.1745–6584.1978.tb03245.x.

Li, B., and T.-C. J. Yeh (1998), Sensitivity and moment analyses of head in variably saturated regimes, *Adv. Water Res.*, *21*(6), 477–485, doi:10.1016/s0309–1708(97)00011-0.

Li, B., and T.-C. J. Yeh (1999), Cokriging estimation of the conductivity field under variably saturated flow conditions, *Water Resour. Res.*, *35*(12), 3663–3674, doi:10.1029/1999WR900268.

Li, W., A. Englert, O. A. Cirpka, J. Vanderborght, and H. Vereecken (2007), Two-dimensional characterization of hydraulic heterogeneity by multiple pumping tests, *Water Resour. Res.*, *43*(4), W04433, doi:10.1029/2006WR005333.

Liu, S., T.-C. J. Yeh, and R. Gardiner (2002), Effectiveness of hydraulic tomography: Sandbox experiments, *Water Resour. Res.*, *38*(4), 1034, doi:10.1029/2001WR000338.

Liu, X., and P. K. Kitanidis (2011), Large-scale inverse modeling with an application in hydraulic tomography, *Water Resour. Res.*, *47*(2), W02501, doi:10.1029/2010WR009144.

Liu, X., W. A. Illman, A. J. Craig, J. Zhu, and T.-C. J. Yeh (2007), Laboratory sandbox validation of transient hydraulic tomography, *Water Resour. Res.*, *43*(5), W05404, doi:10.1029/2006WR005144.

Mao, D., L. Wan, T.-C. J. Yeh, C.-H. Lee, K.-C. Hsu, J.-C. Wen, and W. Lu (2011), A revisit of drawdown behavior during pumping in unconfined aquifers, *Water Resour. Res.*, *47*, W05502, doi:10.1029/2010WR009326.

Mao, D., T.-C. J. Yeh, L. Wan, K.-C. Hsu, C.-H. Lee, and J.-C. Wen (2013a), Necessary conditions for inverse modeling of flow through variably saturated porous media, *Adv. Water Res.*, *52*, 50–61, doi:10.1016/j.advwatres.2012.08.001.

Mao, D., T.-C. J. Yeh, L. Wan, C.-H. Lee, K.-C. Hsu, J.-C. Wen, and W. Lu (2013), Cross-correlation analysis and information content of observed heads during pumping in unconfined aquifers, *Water Resour. Res.*, *49*, 1782–1796, doi:10.1002/wrcr.20066.

Mathias, S. A., and A. P. Butler (2006), Linearized Richards' equation approach to pumping test analysis in compressible aquifers, *Water Resour. Res*, *42*, W06408, doi:10.1029/2005WR004680.

Mishra, P. K., and S. P. Neuman (2010), Improved forward and inverse analyses of saturated-unsaturated flow toward a well in a compressible unconfined aquifer, *Water Resour. Res.*, *46*, W07508, doi:10.1029/2009WR008899.

Moench, A. F. (1995), Combining the Neuman and Boulton models for flow to a well in an unconfined aquifer, *Ground Water*, *33*(3), 378–384.

Neuman, S. P. (1972), Theory of flow in unconfined aquifers considering delayed response of the water table, *Water Resour. Res.*, *8*(4), 1031–1045, doi:10.1029/WR008i004p01031.

Ni, C. F., and T. C. J. Yeh (2008), Stochastic inversion of pneumatic crosshole tests and barometric pressure fluctuations in heterogeneous unsaturated formations, *Adv. Water Res.*, *31*(12), 1708–1718.

Ni, C.-F., T.-C. J. Yeh, and J.-S. Chen (2009), Cost-effective hydraulic tomography surveys for predicting flow and transport in heterogeneous aquifers, *Environ. Sci. Technol.*, *43*(10), 3720–3727, doi:10.1021/es8024098.

Nwankwor, G. I., J. A. Cherry, and R. W. Gillham (1984), A comparativestudy of specific yield determinations for a shallow sand aquifer, *Ground Water*, *22*(6), 764–772.

Russo, D. (1988), Determining soil hydraulic properties by parameter estimation: On the selection of a model for the hydraulic properties, *Water Resour. Res.*, *24*(3), 453–459, doi:10.1029/WR024i003p00453.

Russo, D., and M. Bouton (1992), Statistical analysis of spatial variability in unsaturated flow parameters, *Water Resour. Res.*, *28*(7), 1911–1925.

Srivastava, R., and T.-C. J. Yeh (1992), A three dimensional numerical model for water flow and transport, *Adv. Water Res.*, *15*, 275–287.

Straface, S., T.-C. J. Yeh, J. Zhu, S. Troisi, and C.-H. Lee (2007), Sequential aquifer tests at a well field, Montalto Uffugo Scalo, Italy, *Water Resour. Res.*, *43*, W07432, doi:10.1029/2006WR005287.

Streltsova, T. D. (1972a), Unsteady radial flow in an unconfined aquifer, *Water Resour. Res.*, *8*(4), 1059–1066.

Streltsova, T. D. (1972b), Unconfined aquifer and slow drainage, *J. Hydrol.*, *16*(2), 117–124, doi:10.1016/0022–1694(72)90117-5.

Stüben, K., and T. Clees (2010), *SAMG User's Manual*, Fraunhofer Inst. SCAI, Sankt Augustin, Germany.

Theis, C. V. (1935), The relation between the lowering of the piezometric surface and the rate and duration of discharge of a well using ground water storage, *Trans. Am. Geophys. Union*, *16*, 519–514.

Wen, J.-C., C.-M. Wu, T.-C. J. Yeh, and C.-M. Tseng (2010), Estimation of effective aquifer hydraulic properties from an aquifer test with multi-well observations (Taiwan), *Hydrogeol. J.*, *18*(5), 1143–1155, doi:10.1007/s10040-010-0577-1.

Wu, C.-M., T.-C. J. Yeh, J. Zhu, T.-H. Lee, N.-S. Hsu, C.-H. Chen, and A. F. Sancho (2005), Traditional analysis of aquifer tests: Comparing apples to oranges, *Water Resour. Res.*, *41*, W09402, doi:10.1029/2004WR003717.

Xiang, J., T.-C. J. Yeh, C.-H. Lee, K.-C. Hsu, and J.-C. Wen (2009), A simultaneous successive linear estimator and a guide for hydraulic tomography analysis, *Water Resour. Res.*, *45*(2), W02432, doi:10.1029/2008WR007180.

Yeh, T.-C. J., and C.-H. Lee (2007), Time to change the way we collect and analyze data for aquifer characterization, *Ground Water*, *45*(2), 116–118, doi:10.1111/j.1745–6584.2006.00292.x.

Yeh, T.-C. J., and S. Liu (2000), Hydraulic tomography: Development of a new aquifer test method, *Water Resour. Res.*, *36*(8), 2095–2105, doi:10.1029/2000WR900114.

Yeh, T.-C. J., and J. Zhu (2007), Hydraulic/partitioning tracer tomography for characterization of dense nonaqueous phase liquid source zones, *Water Resour. Res.*, *43*, W06435, doi:10.1029/2006WR004877.

Yeh, T.-C. J., L. W. Gelhar, and A. L. Gutjahr (1985a), Stochastic analysis of unsaturated flow in heterogeneous soils: 1. Statistically isotropic media, *Water Resour. Res*, *21*(4), 447–456.

Yeh, T.-C. J., L. W. Gelhar, and A. L. Gutjahr (1985b), Stochastic analysis of unsaturated flow in heterogeneous soils: 2. Statistically anisotropic media with variable $\alpha$, *Water Resour. Res.*, *21*(4), 457–464.

Yeh, T.-C. J., L. W. Gelhar, and A. L. Gutjahr (1985c), Stochastic analysis of unsaturated flow in heterogeneous soils: 3. Observations and applications, *Water Resour. Res.*, *21*(4), 465–471.

Yeh, T.-C. J., M. Jin, and S. Hanna (1996), An iterative stochastic inverse method: Conditional effective transmissivity and hydraulic head fields, *Water Resour. Res.*, *32*(1), 85–92, doi:10.1029/95WR02869.

Yeh, T.-C. J., D. Mao, L. Wan, C.-H. Lee, J.-C. Wen, and K.-C. Hsu (2011), Well definedness, scale consistency, and resolution issues in groundwater model parameter identification, Rep., Univ. of Arizona, Tucson, HWR 2011-010.

Yeh, T. C. J., D. Mao, L. Wan, C. H. Lee, J. C. Wen, and W. Lu (2012), Replies to comments on ''A revisit of drawdown behavior during pumping in unconfined aquifers'' by Neuman and Mishra, *Water Resour. Res.*, *48*(2), W02802, doi:10.1029/2011WR011153.

Yin, D. T., and W. A. Illman (2009), Hydraulic tomography using temporal moments of drawdown recovery data: A laboratory sandbox study, *Water Resour. Res.*, *45*, W01502, doi:10.1029/2007WR006623.

Zhu, J., and T.-C. J. Yeh (2005), Characterization of aquifer heterogeneity using transient hydraulic tomography, *Water Resour. Res.*, *41*, W07028, doi:10.1029/2004WR003790.

Zhu, J., and T. C. J. Yeh (2006), Analysis of hydraulic tomography using temporal moments of drawdown recovery data, *Water Resour. Res.*, *42*(2), W02403, doi:10.1029/2005WR004309.

Zhu, J., and T.-C. J. Yeh (2008), Hydraulic tomography to characterization of heterogeneity of unconfined aquifers, paper presented at AGU Fall Meeting, San Francisco, Calif.

Zhu, J., T.-C. J. Yeh, and D. Mao (2011), Hydraulic tomography to characterize heterogeneity of unconfined aquifers, *J. Nanjing Univ.*, *47*(3), 252–264.